Modeling of Epoxy Resin Spacers for the 1 MV DC Gas Insulated Line of ITER Neutral Beam Injector System

A. De Lorenzi, L. Grando, A. Pesce
Consorzio RFX.
Corso Stati Uniti, 4, 35127, Padova, Italy

P. Bettini and **R. Specogna**
DIEGM, Università di Udine,
Via delle Scienze, 208, I-33100 Udine, Italy

ABSTRACT

The spacers for the Gas Insulated Transmission Line for the ITER neutral beam injector will be designed to withstand the operating voltage of 1 MV dc. Electric charging processes of the spacer surface are then expected to play an important role in the final electric field distribution. Aim of the paper is to investigate the effects of the different conductivity properties of the SF6-Spacer insulating structures on the surface charge set-up, and to identify a procedure to minimize this charge. Based on the most updated literature, the paper presents and discusses the results of two newly developed simulation tools: the first consisting of a quasi-static non linear model for epoxy spacer based on finite element method code ANSYS™, the other consisting of a spacer profile optimization package, whose kernel is based on a genetic algorithm. The numerical tools have been applied to post and disk spacer models of the gas insulated line; in particular, the optimization package has been used on the disk spacer, and the comparison between un-optimized and optimized spacer in terms of electric charge accumulated are presented and discussed.

Index Terms — **Neutral Beam Injector, HVDC insulation, epoxy resin insulator, surface charging, triple-junction, optimization method.**

LIST OF SYMBOLS

σ	surface charge density
E_n,	electric field component normal to the insulator;
E_t	electric field component tangential to the insulator surface,
γ_i	bulk insulator conductivity
γ_g	gas conductivity
γ_s	insulator surface conductivity
ε_g	gas permittivity
ε_i	bulk insulator permittivity
j_s	surface current density
U_b	50% probability breakdown voltage

1 INTRODUCTION

IN the framework of the International Thermonuclear Experimental Reactor (ITER) project [1] supported by EU, Japan, Russian Federation, USA, China, South Korea and India, the design of a full scale prototype of the 40 MW Neutral Beam Injector for Plasma Heating and Current Drive has begun.

This system shall produce a 40A Negative Ion Beam (NIB) of Deuterium, accelerated by -1 MV voltage between the Ion Source polarized at negative voltage and the grounded grid; the NIB is then neutralized to obtain an energetic (1MeV) Deuterium atoms beam, transferring power (approx 16 MW) and momentum to the ITER thermonuclear plasma.

Figure 1 sketches the NBI electrical circuit scheme.

The Acceleration Grid Power Supplies (AGPS) for the beam acceleration are composed of five equal sections each formed by an ac-ac converter, step-up transformer and rectifying diode bridge rated for 200 kV output voltage. The units are connected in series to obtain -1 MV; the step-up transformer insulation to ground and between LV and HV windings is rated for 1 MV dc.

The Negative Ions are produced by the Ion Source Power Supplies (ISPS), a low voltage-high current system biased at -1MV potential installed in an air-insulated platform and fed by a 1MV insulating transformer [2].

The power is transmitted by a 75 m long coaxial Gas Insulated Transmission Line (GITL) which is one of the most critical components for the reasons discussed hereinafter.

Firstly, nowadays a HVDC GIL-GIS design with the same reliability degree of corresponding HVAC systems remains a challenge; in our case, the GITL shall operate at -1MV, a value twice the ±500 kV dc value of Kii (Japan) HVDC GIS rated voltage [3], and twice the worldwide highest rated voltage of the -500 kV Negative Ions NBI GITL installed in the Japanese Fusion Machine JT-60 [4].

Manuscript received on 6 August 2008, in final form 26 September 2008.

Secondly, due to the peculiar operation of the NBI systems, the voltage frequently (0.1-0.5 Hz) collapses due to breakdowns across the accelerating gap, and recovers in few tens of ms [5]; AGPS internal breakdown will produce instead a fast transient voltage reversal of the order of 50%. Transient 1.3 p.u.(per unit) over-voltages (max 1s) will seldom occur (depending on mis-operation of the AGPS) and no fast transient overvoltages are expected.

Thirdly, the terminal GITL section (close to the Injector) shall operate in an ionizing radiation environment due to the fusion reaction byproducts occurring inside the ITER plasma; such radiation is expected to enhance the SF6 conductivity [17].

The literature clearly indicates that an important - and specific - issue for the HVDC Gas Insulated Devices is the electric charge density which accumulates on the separation surface between gas and solid insulators; the other crucial issue for the insulation stability -the presence of metal particles inside the GITL- can be faced taking advantage of the long term experience gained on HVAC GIS, addressed to reduce the dimension of residual particles below 2-3 mm, to realize electrostatic traps and to avoid particle levitation [6]. The absence of impulse voltages during the NBI operation greatly reduces the risk of metal particle induced breakdown, so that the metal particle problem is not the prevailing aspect in the NBI GITL design, like in [7], [8].

Therefore, the NBI GITL spacer design is addressed to the surface charge density minimization. In fact, charge accumulation has the macroscopic effect of reducing the 50% probability breakdown voltage; this effect takes place through the U-T relationship [9]:

$$U_b(t) = U_b(t_0)\cdot\left(\frac{t}{t_0}\right)^{-\frac{1}{m}} \quad t < t_f \qquad (1)$$

$$U_b(t) = U_{bs} \quad t > t_f$$

where t_f is the time instant related to the completion of the surface charging processes occurring at the spacer surface and $U_b(t_0)$ is the 50% probability breakdown voltage after 1 min from voltage application, when the spacer charge is still zero, corresponding to the capacitive field distribution. There is experimental evidence that lower breakdown voltages U_{bs} (lower m values) correspond to larger surface charge densities.

This effect has been explained [11] as follows: a localized discharge, which in pure gas remains stabilized, in presence of charge density can propagate due to ionization processes fed by the surface energy density associated to the surface charge. Experiments showed that the phenomenon occurs when the surface energy density exceeds a certain limit, of the order of 0.1 J/m^2/MPa; it is interesting to observe that such limit can be reached when the applied voltage collapses to zero.

Aim of the paper is to present and discuss the design tools developed on one hand to evaluate surface charge accumulated on the spacers and the associated electric field, on the other hand to optimize the spacer profile to reduce the surface charge. The first tool, described in Par. 2, consists of an Electro Quasi Static (EQS) - non linear model of epoxy spacer using ANSYS™, based on a non linear transient procedure implementing an iterative technique to account for the modification of the spacer surface conductivity; the second tool, described in Par. 3, consists of a spacer shape optimizer, devoted to minimize a given objective function, defined as a combination of electric field and its spatial derivative in the electrostatic distribution.

These tools have been applied to the two typologies of spacers installed inside the NBI Transmission Line: a post spacer supporting the high voltage inner conductor and a disk spacer acting as gas-tight barrier (see Figure 1); first, a parametric analysis of the post spacer (non optimized) has been carried out in order to quantify the dependence of surface charge distribution on the conductivities and non linearity of the media. Second, the computations are applied to the disks spacer, whose shape has been subjected to the optimization tool and then the resulting electric field and charge density profiles are compared between non optimized and optimized shapes.

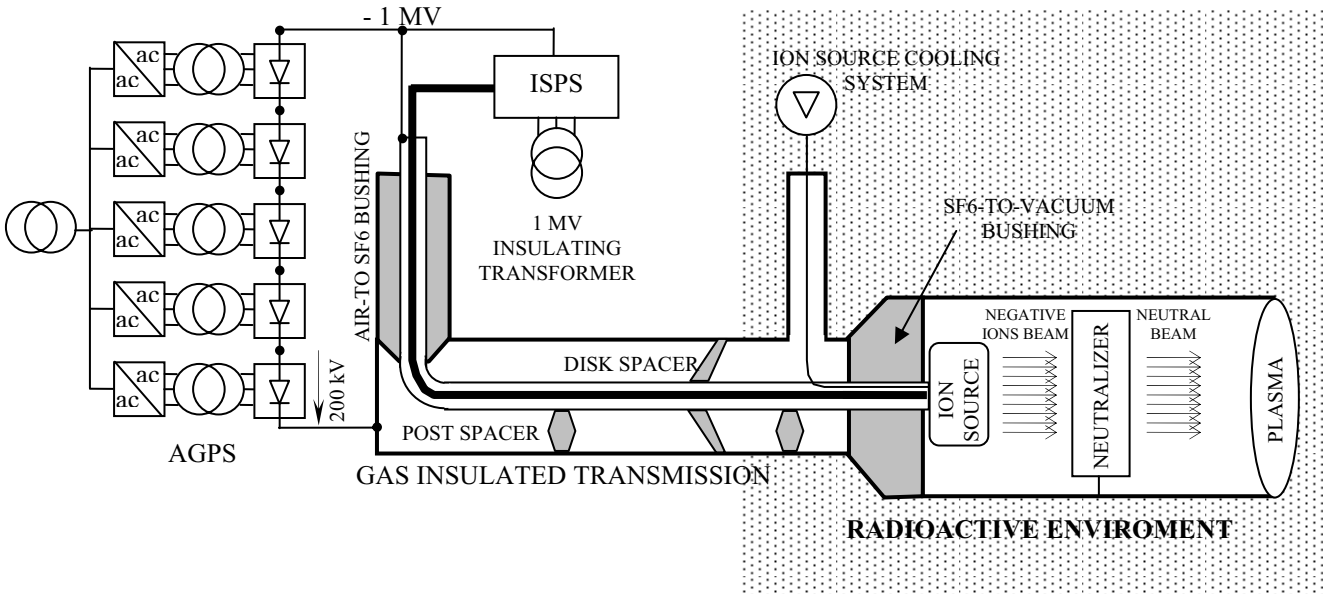

Figure 1. Schematic of the Neutral Beam Injector structure.

The size of the post and disk spacers are related to a coaxial line whose inner conductor diameter is D_{int}= 400 mm, needed to host the cumbersome conductor system of the ISPS feeding the ion source (see Figure 1); the electric field at the inner conductor surface has been set to 5 MV/m at 1MV. Using the minimum volume criterion ($D_{ext}/D_{int} = e = 2.718$), the external diameter results D_{ext}=1100 mm. The electric field at the ground electrode results 1.84MV/m. At 0.3 MPa in SF6 these electric field values are considered safe against gap breakdown and particle levitation (provided the ground electrode has a dielectric coating [6]).

2 ELECTRO QUASI STATIC - TIME VARIANT MODEL

2.1 GENERAL DESCRIPTION

The spacer surface charging process is described by equation (2):

$$\frac{d\sigma}{dt} = \gamma_i \cdot E_{in} - \gamma_g \cdot E_{gn} - \nabla \cdot \left(\gamma_s \cdot E_\tau\right) \qquad (2)$$

which accounts for two mechanisms of charge accumulation: the first term is the commonly recognized mechanism of charging driven by the normal component of electric field and the second term is the surface current density gradient, a less known mechanism for charge accumulation, highlighted in literature by [9, 10].

The order of magnitude of the time constant governing the transition from the capacitive to resistive distribution can be evaluated using the following approximate formula which depends also on the size of the spacer:

$$T = \frac{\varepsilon_g + \varepsilon_i}{\gamma_g + \gamma_i + \gamma_s / R_0} \qquad (3)$$

where R_0 is the characteristic dimension of the insulating system [15]. Table 1 reports the values of the SF6 and epoxy resin parameters which can be applied to our case. Such large variation in the conductivity value has a strong impact on the transition time constant, which can range from some minutes to some days, and on the surface charge density, which, for example, can have either homo-charge or hetero-charge distribution.

Table 1. Values of the cast epoxy resin and SF6.

Parameter	Epoxy Resin	SF6
ε_r	4-5	1
γ_i	10^{-19}-10^{-12} [S/m]	10^{-20}-10^{-16} [S/m]
γ_s	10^{-20}-10^{-17} [S]	-

The bulk epoxy resin and the surface conductivities show a dependence on both electric field and temperature, expressed by

$$\gamma = \gamma_0 \cdot e^{\alpha \cdot |E| + \beta \cdot T} \qquad (4)$$

where the surface and bulk conductivities are [10, 14, 12]

$1.2<\alpha<1.4$ mm·kV^{-1}, β=0.05 C^{-1}, $10^{-20}<\gamma_0<10^{-19}$ S (surface)

α=0.08 mm·kV^{-1}, β=0.1 C^{-1}, $10^{-20}<\gamma_0<10^{-14}$ S/m (bulk).

In our case the temperature is kept under control, so that the bulk conductivity remains almost constant (depends weakly on electric field) and its value can be controlled by the manufacturing procedure (e.g. using a filler); instead surface conductivity strongly depends upon tangential electric field and such non-linearity must be taken into account; again, the treatment of the spacer surface by semi-resistive coating or by mechanical processes can be considered to control the surface conductivity.

The large variation of the SF6 conductivity is peculiar for the ITER NBI installation, due to the presence of radio-active environment (see Figure 1) for part of the Transmission Line: in fact, γ and X radiation induces a several order of magnitude enhancement of SF6 conductivity [5, 17, 18 and 19].

In order to asses the effects on charging processes, in our case it is then necessary to implement a spacer model capable of evaluating the time evolution of charge density and electric field, in presence of the non linear behavior of surface conductivity.

2.2 MODEL IMPLEMENTATION

The interface between epoxy resin and gas has been modeled by a layer whose thickness is much smaller than the dimensions of the other insulating media.

In this way the insulating system consists of three finite regions (SF6, bulk insulator and layer) where the following equation describes the time evolution of the electric scalar potential V:

$$\nabla \cdot \left(\gamma \cdot \nabla V\right) + \nabla \cdot \left(\varepsilon \cdot \nabla \frac{\partial V}{\partial t}\right) = 0 \qquad (5)$$

The ANSYS code is able to solve equation (5) in the linear case; for the solution two different 2-D 8-node elements, based on the electric scalar potential formulation, were adopted: PLANE121 for the electrostatic analysis and PLANE230 for the current conduction analysis.

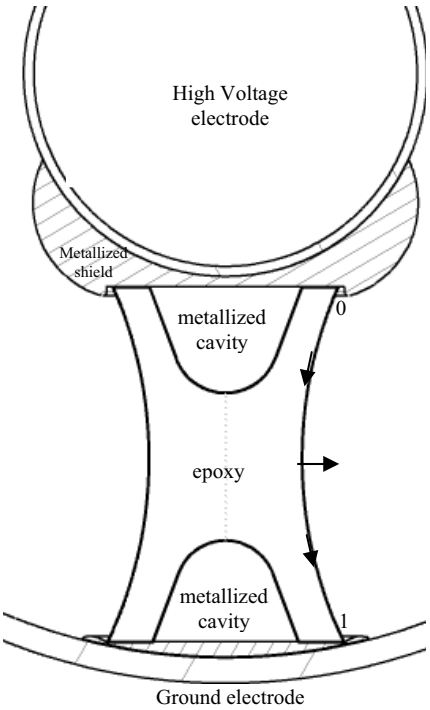

Figure.2. Post spacer shape. Arrows indicate positive direction of tangential and normal electric field.

In order to take into account the non linearity introduced by equation (4), the procedure adopted is the following.

First, the surface conductivity γ_s is transformed into a volume conductivity γ_s^* by means of

$$\gamma_s^* = \frac{\gamma_0 \cdot e^{\alpha \cdot |E\tau|}}{\delta} \tag{6}$$

where δ is the virtual thickness of the surface layer. In this way a mesh for the Finite Element Method (FEM) solution made by surface elements is obtained; the δ thickness value adopted (100 μm) is a compromise between the need to keep the surface mesh elements of a reasonable size (and number), and to guarantee that the surface normal component of the displacement vector D_n and of the current density J_n do not vary appreciably along the layer thickness. It must be underlined that such thickness is not related to the actual surface thickness - sub micron range - in which surface phenomena take place [14].

Second, for each k^{th} time step Δt the ANSYS solver finds the electric potential distribution solving equation (5), considered linear within the time Δt; once found the V_k and $\mathbf{E}_k$ distribution , an external routine computes the electric field tangential to the spacer surface in order to evaluate the new value of the surface conductivity $\gamma^*_{s,k}$ by equation (6); the V_{k+1} distribution is then found as the solution of equation (5) using as initial condition the V_k distribution in the presence of the new conductivity $\gamma^*_{s,k}$

$$V_{k+1} \leftarrow V_k\left(\gamma^*_{s,k}\right) \tag{7}$$

The time step Δt is fixed or is a function of the time constant given by equation (3).

spacer, whose shape (see Figure 2) is derived from [9] and adapted to the cylindrical geometry of the GITL. The shape has not been optimized as far surface charge and electric field distribution are concerned. The problem geometry is two-dimensional, representing the transverse section of the line, assuming infinite length along z axis.

Table 2 summarizes the cases studied, covering all the possible operating conditions, including also the effects of some manufacturing processes of the spacer aimed to control the surface electric field.

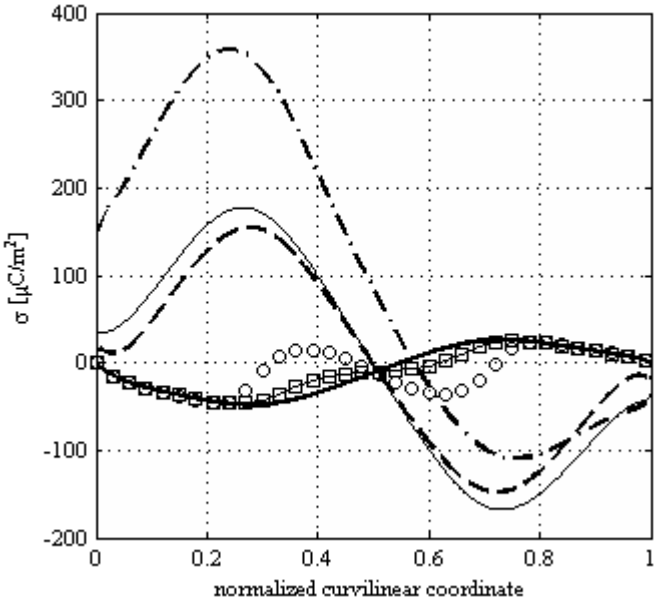

Figure 3. Surface charge density along the interface between spacer and SF_6 gas. Case 1 bold solid line; case 2 solid line; case 3 dashed line; case 4 circle; case 5 square line; case 6 dash-dot line.

Table 2. Cases studied.

Case	Surface layer	SF_6 [S/m] $\varepsilon_r = 1$	Bulk [S/m] $\varepsilon_r = 4$	Layer ($\varepsilon_R = 4$)	
				γ_0 [S]	α
1	Absent	10^{-20}	$3.5 \cdot 10^{-15}$	--	--
2	Present - γ linear (coating)	10^{-20}	$3.5 \cdot 10^{-15}$	10^{-6}	0
3	Present - γ non linear	10^{-20}	10^{-18}	10^{-20}	1.48
4	Present - γ non linear surface untreated	10^{-20}	$3.5 \cdot 10^{-15}$	10^{-20}	1.48
5	Present - γ non linear surface horned	10^{-20}	$8 \cdot 10^{-15}$	10^{-19}	0.83
6	Absent RIC	10^{-15}	10^{-18}	--	--

The accumulated surface charge density (σ) is calculated for each point of the interface between gas and spacer by post processing the final solution; the accuracy of the solution has been evaluated comparing the values of the surface charge calculated by Gauss's law

$$\sigma(t) = \varepsilon_g \cdot E_{gn}(t) - \varepsilon_i \cdot E_{in}(t) \tag{8}$$

or by integrating equation (2).

This procedure has been benchmarked with analytical reference problems and cases studied using different codes [15].

2.3 POST SPACER MODEL

The study of the parameters governing the surface charge and electric field distribution has been carried out on a post

Case 1 (spacer uniform conductivity) represents the ideal case for dc voltage application. Case 2 is representative of the electric field control technique based on surface painting using some kind of semi-conductive varnish. Cases 3, 4 and 5 are relevant to a more realistic condition of the epoxy spacer, in which the surface conductivity is dominated by surface state (humidity, pollution), leading to the conductivity exponential dependence on tangential electric field described by equation (6); in particular, cases 4 and 5 have been kept from [10]. Case 6 accounts for a very specific operating condition of the ITER NBI system: the last section of the GITL is immersed in

a radioactive environment (typically γ and x); the radiation enhances the SF6 conductivity (Radiation Induced Conductivity (RIC) effect [17, 18]) even in the presence of relatively low radiation dose rates.

2.3.1 RESULTS OF THE ANALYSIS

Figure 3 reports the charge distribution accumulated along the spacer surface, once the electric field has relaxed to its final resistive distribution, for cases of Table. 2.

For reference case 1 (isotropic bulk conductivity and layer absent), a maximum charge density of about 40 μC/m^2 is accumulated on the interface surface with homo-charge distribution. When a surface current density is generated due to the effect of a layer conductivity increase, the hetero-charge distribution starting from the middle of the spacer appears. The hetero-charge distribution prevails as long as the surface current conduction becomes predominant with respect to the bulk current. For cases with non linear surface conductivity (cases 3, 4 and 5) the charge accumulation is reduced by a mechanical surface treatment (horned surface), because it

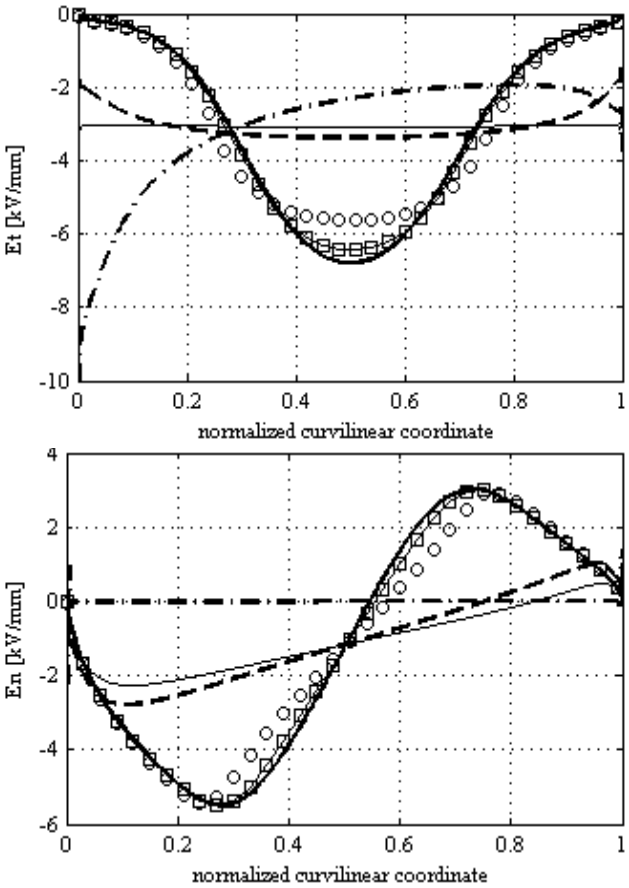

Figure 4. Normal and tangential electric field along post spacer surface and time evolution of the total charge
Case 1 bold solid line; case 2 solid line; case 3 dashed line; case 4 circles; case 5 squares; case 6 dash-dot line

reduces the non-linear effect. Of particular interest is the case of a treatment with a semi-conductive coating (case 2): a hetero-charge distribution with a maximum charge density of 180 μC/m^2 is generated, much larger than the uniform case.

Case 6 shows a charge distribution different from cases 1-5, being not symmetric with respect to the curvilinear abscissa and with a huge peak of hetero-charge density. These results can be qualitatively explained, according to equation (2). The rate of charge accumulation on the insulator surface comes from two contributions: one is the current density driven by the normal field, the other is given by the gradient of the current flowing along the spacer surface, driven by the tangential field; clearly, these field components correspond, at t=0, to the electrostatic distribution (pure capacitive). The homo-charge accumulated in the reference case 1 is mostly produced by the normal field component inside the spacer, since the epoxy conductivity greatly exceeds the SF6 one; for cases 2-5, hetero-charge driven by surface current gradient adds to the homo-charge distribution, becoming predominant for cases 2 and 3. Case 6 is, in some way, the dual of case 1, being the SF6 conductivity much larger than epoxy one; but in

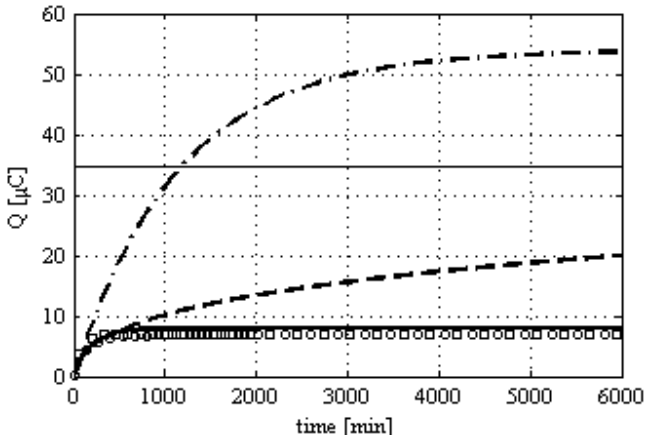

Figure 5. Time evolution of the electric charge (absolute value)
Case 1 bold solid line; case 2 solid line; case 3 dashed line; case 4 circles; case 5 squares; case 6 dash-dot line.

this case the electric charge is much larger, because of the difference between the electric field normal components at epoxy and SF6 sides.

The reduction of the electric charge accumulation then becomes a quite complicated task, because it requires the optimization of the spacer shape to reduce not only the normal component of the electric field, but also the tangential component and its spatial derivative.

Figure 4 reports the final (resistive) distributions of the tangential and normal electric field for cases 1-6. From comparison between cases 1, 4 and 5, the beneficial effect of non linearity is evident, owing to the reduction of the tangential electric field in the middle of the spacer, whilst in the triple-junctions the electric field remains practically zero; the normal field component is almost unchanged. In cases 2 and 3 instead, where the surface conductivity dominates, a remarkable flattening of tangential field occurs (for the extreme case 2: E_t=const.), leading to an unwelcome increase of the tangential field at the triple-junctions; correspondingly, there is a reduction of the normal field. Finally, in case 6 the huge charge accumulation leads to an unacceptable increase of tangential field, having its maximum at the triple-junction at high voltage electrode; the normal component is zero, because of the total screening effect of the electric charge accumulated

Figure 5 shows the time evolution of the absolute value of total accumulated electric charge per unit length of the spacer; the total charge accumulated and the time constants for the reference cases are summarized in Table 3.

Table 3. Time constants and Charges for cases studied

Case	charge [μC]	$T_{analysis}$ [min]	$T_{[eq. 3]}$ [min]
1	8	195	211
2	35	--	--
3	40	2610	21700
4	6.8	148	210
5	6.9	82	92
6	54	1144	737

The time constant relevant to the FEM analysis has been computed as the time to reach the 63% of the final value.

The set-up time constant greatly varies and a reasonable agreement is achieved between results from FEM analysis for cases 1, 4, 5 and equation (3); for case 3, the difference is large due to the strong non linearity; also in case 6, where the SF6 conductivity dominates, the agreement between model results and equation (3) is poor.

3 DISK SPACER PROFILE OPTIMIZATION

The previously described analyses showed how strong is the dependence of accumulated electric charge on conductivity parameters and, correspondingly, of the electric field final distribution. As stated in [9, 16], the optimization of the shape would be then addressed to obtain an "anti-charging" spacer. The approach followed is to minimize the second term of equation (2), for t=0, i.e. keeping as low as possible the normal component and the spatial derivative of the tangential component of the electrostatic (capacitive) distribution along the spacer surface.

Hereafter we will apply to the disk spacer described in [5] such optimization criterion by the use of the following shape optimization procedure.

3.1 GENERAL DESCRIPTION

Computational design optimization of electromagnetic structures with respect to their geometrical and electrical parameters is a demanding task, even using last generation computers. On the one hand, the function to be optimized is unknown and, consequently, it is necessary to calculate many solutions to reach a sub-optimal one. On the other hand the evaluation of each solution requires a high computational cost. Therefore, the development of a suitable procedure, that has to be robust and fast enough is of paramount importance.

An optimization package has been developed and applied to the design of the epoxy resin disc spacer, under electrostatic conditions. This package consists of four main tools: a parametric CAD pre-processor (*mesh generator*), an electrostatic field solver (*analysis tool*), a numerical optimization algorithm (*search tool*) and a *post-processor* for optimized model analysis.

Simulated Annealing (SA) and Genetic Algorithms (GAS) are the search techniques most widely used to optimize multimodal functions, namely functions with many minima, typical of electromagnetic design problems. Furthermore, GAS seem well suited for the problem at hand, because they can span large

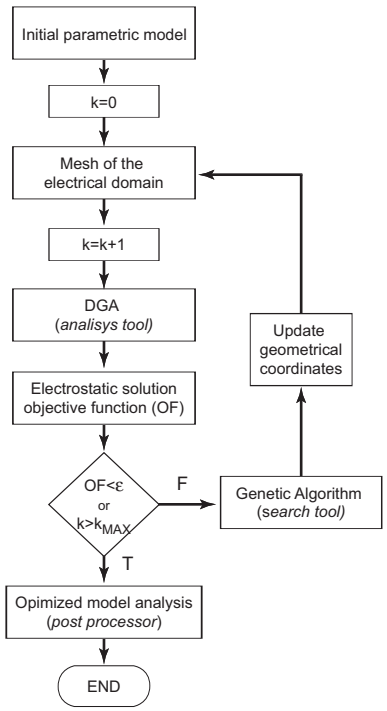

Figure 6. Optimization procedure flow chart.

solution spaces and are suitable for a full exploitation of parallelism due to their intrinsically parallel structure. Therefore, a Genetic Algorithm (GA) has been developed to play the role of *search tool* [20, 21]. The *analysis tool* is based on a Discrete Geometric Approach (DGA) for the solution of electrostatic field problems [22, 23]. The optimization procedure is hereafter described. Figure 6 shows its flow chart.

The initial model is prepared using geometric data, material properties and boundary conditions (BCs). The optimization (design) variables are specified as a set of parameters of the geometric model, with appropriate upper and lower bounds to account for physical constraints. As each point in the search space represents a different design, the GA submits that particular design to the *mesh generator* which automatically regenerates the geometric model.

Then the *analysis tool* solves the (2D axi-symmetric) electrostatic field equations for the submitted design and returns the relevant parameters (*objective function (OF) value*) back to the *search tool* until a stop condition is reached (minimum tolerance ε or maximum number of iterations k_{MAX} exceeded). Finally, the *post-processor* runs a standard analysis of the optimized model.

Clearly, different versions of GAs with different performances can be synthesized by modifying either the algorithm itself or its functions. The representation scheme itself, i.e. the way the design variables are coded into *chromosomes* (finite-length character strings), is a crucial point. In the present GA the *Gray coding* is adopted as representation scheme and the three fundamental operators (reproduction, crossover, mutation), are introduced with an advanced selection scheme. The choice of GA's parameters is user and problem dependent and directly affects the performance of the GA.

In this case, the main parameters have been set as follows:
M (number of chromosomes in each population): 50
N (number of iterations): 250
a (accuracy): 0.1mm
$\mathbf{p_c}$ (crossover probability): 0.75
$\mathbf{p_m}$ (mutation probability): 0.01

It must be pointed out that the choice of the values of GA's parameters, **M** and **N** in particular, is a trade-off between speed and accuracy of the optimal design procedure. In the design of the epoxy resin disc spacer, a multi-objective optimization problem has to be solved, where different requirements, corresponding to different objective functions (e.g. normal field, tangential field, spatial derivatives on the upper and lower surfaces of the disc), have to be fulfilled at a time. Therefore a *vectorial* optimization takes place, namely a problem characterized by a vector of objectives simultaneously depending on a set of design variables. In the present algorithm, the *Method of Objective Weighting* is adopted, to transform the *vectorial* problem into a *scalar* one,

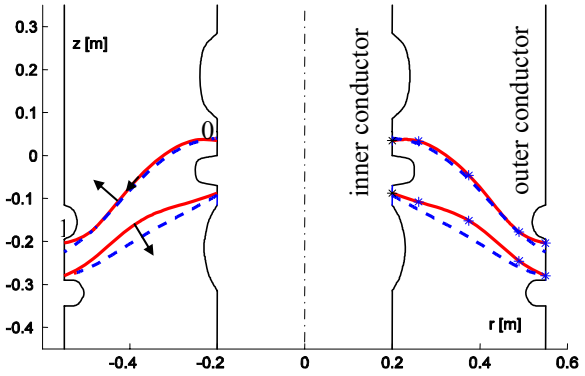

Figure 7 Contours of the axial cross-section: optimized (solid), reference (dashed). * symbols represent the *key points* of the mesh. Arrows indicate positive direction of tangential and normal electric field

by means of a linear combination of the different objective functions into a new cost function defined as *global performance* function. The choice of the coefficients of the linear combination is again user dependent and strongly affects the behaviour of the GA. The best individual, throughout all reproduced generations, is selected as the optimal solution.

In the overall procedure, the evaluation of the *fitness measure* of each individual (decoded chromosomes) is the most time consuming task, due to the numerical computations required by both the *mesh generator* and *analysis tool:* about 15 s of CPU time are needed for each evaluation, even using efficient Fortran codes on last generation computers. In the proposed algorithm, some CPU time is saved at this stage, by keeping record of the previous generation's chromosomes and their fitness measures. If some chromosome also appear in the new generation, then its fitness measure is already known.

The OF has the form:

$$OF = \sum_i k_i f_i, \quad \sum_i k_i = 1 \tag{9}$$

where f_i are normalized functions (between 0 and 1) of tangential (E_t) and normal (E_n) components of the electric field and E_t derivative ∇E_t calculated in points laying on upper and lower surfaces of the spacer. The following upper bounds have been adopted for electrical field and its gradient components: $E_t < 3.5$ kV/mm, $E_n < 3.5$ kV/mm, $\nabla E_t < 0.2$ kV/mm^2.

3.2 OPTIMIZATION RESULTS

This optimization package has been applied to the design of the epoxy resin disc spacer presented in Figure 7. The 2D profiles (axial cross-section) for the optimized configuration (solid line) is presented together with the 2D profiles of the reference configuration (dashed line). The reference configuration has the same disk profile presented in [5]; this reference profile is the result of the optimization procedure employing the *direct search optimization method* algorithm [24]; the shapes of the triple-junction screens have been instead modified to obtain a more realistic condition.

The geometry of the problem has been described in the CAD pre-processor only by straight lines and *natural cubic splines*. The design variables are the vertical coordinates *z* of 10 *key points* of the mesh (5 on upper profile, 5 on lower profile of the disc spacer) at the same fixed radial coordinates *r* (see symbols

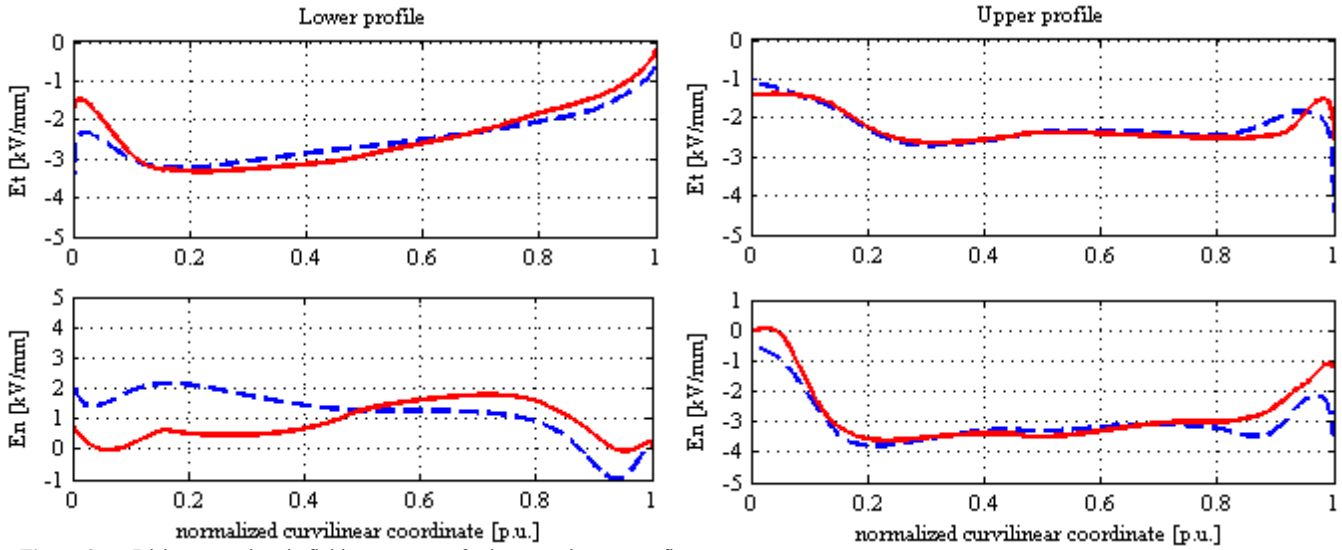

Figure 8 Disk spacer electric field components for lower and upper profiles. Solid line: optimized configuration; dashed line: reference configuration.

"*" in Figure 7). Once the optimization procedure had been completed, the triple-junction electric field refinement was obtained by hand.

The optimization procedure has mainly modified the lower profile, the upper remaining almost unchanged.

In Figure 8 the electric field components of the optimized spacer are compared to the reference spacer, along both profiles. The electric field module (|E|) evaluated at internal and external triple-junctions (metallic electrode – SF6 gas – solid insulator) are indicated in Table 4.

Table 4. Electric field components at triple-junctions

Position	|E| optimized [kV/mm]	|E| reference [kV/mm]
Lower internal	2.0	3.2
Lower external	0.2	0.8
Upper internal	1.5	1.1
Upper external	2.7	5.5

Clearly, since the upper surface is slightly modified, both E_t and E_n components have only small changes. It can be only observed a flattening on the E_t shape, effect of the minimization of the spatial gradient. It must be underlined that the optimization procedure lowered also the electric field at the triple-junction, but it has been found that with manual refinement the electric field can be further reduced (see Table 4). The normal component, instead, slightly decreased along the whole upper surface.

3.2.1 EFFECT ON CHARGE ACCUMULATION

Simulations on the two disk spacer profiles (reference and optimized) have been carried out through the cases reported in

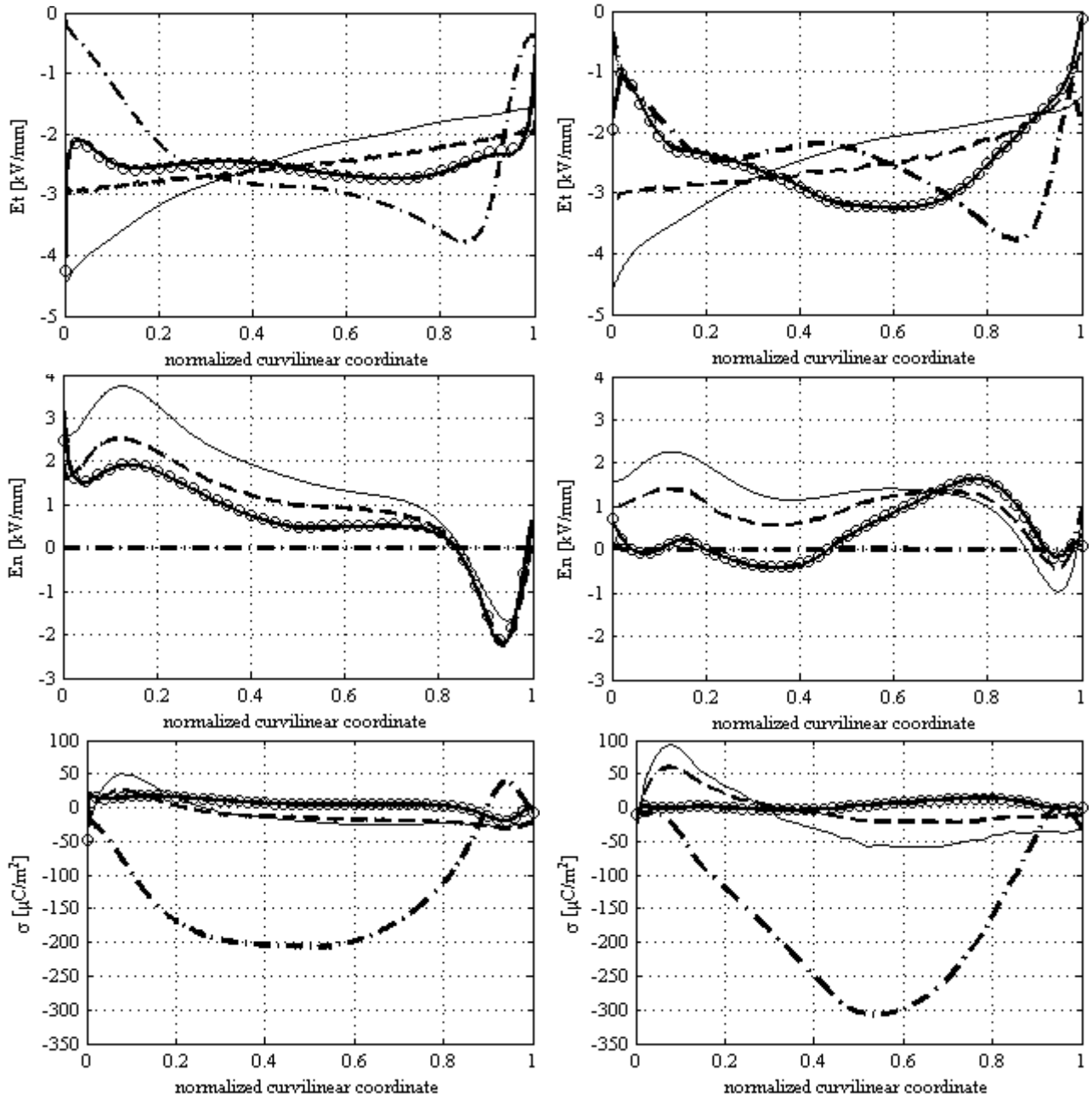

Figure 9. Comparison between reference spacer –left- and optimized spacer – right; lower surface

Case 1 Bold solid line, Case 2 solid line, Case 3 dashed line, Case 4 circle, Case 6 dash-dot line.

Table 2, aimed to assess how the profile optimization reflects in the dc (resistive) electric field and surface charge distribution. Figures 9 and 10 report the comparison for the lower and upper surfaces respectively. Case 5 has been skipped, being the relevant distributions superposed to those of case 4. The observations on the results are summarized as follows.

3.2.1.1 LOWER SURFACE

- Effects on electric field.
  - The reduction of normal field is maintained (and even improved) in the resistive distribution relevant to cases 1 and 4. An improvement is obtained also for cases 2 and 3, with a reduction of the peak value. Clearly, the normal electric field for case 6 is zero because of the high conductivity of the SF6.
  - The tangential electric field for cases 1 and 4 for the optimized profile is lower than the reference close to the inner conductor, so leading to a moderate increase in the central area. No effect of the optimization are found for cases 2, 3 and 6.
- Effects on accumulated charge.
  - For cases 1 and 4 the surface charge density is further reduced, in particular close to the outer (grounded) conductor. For all other cases the electric charge density increases.

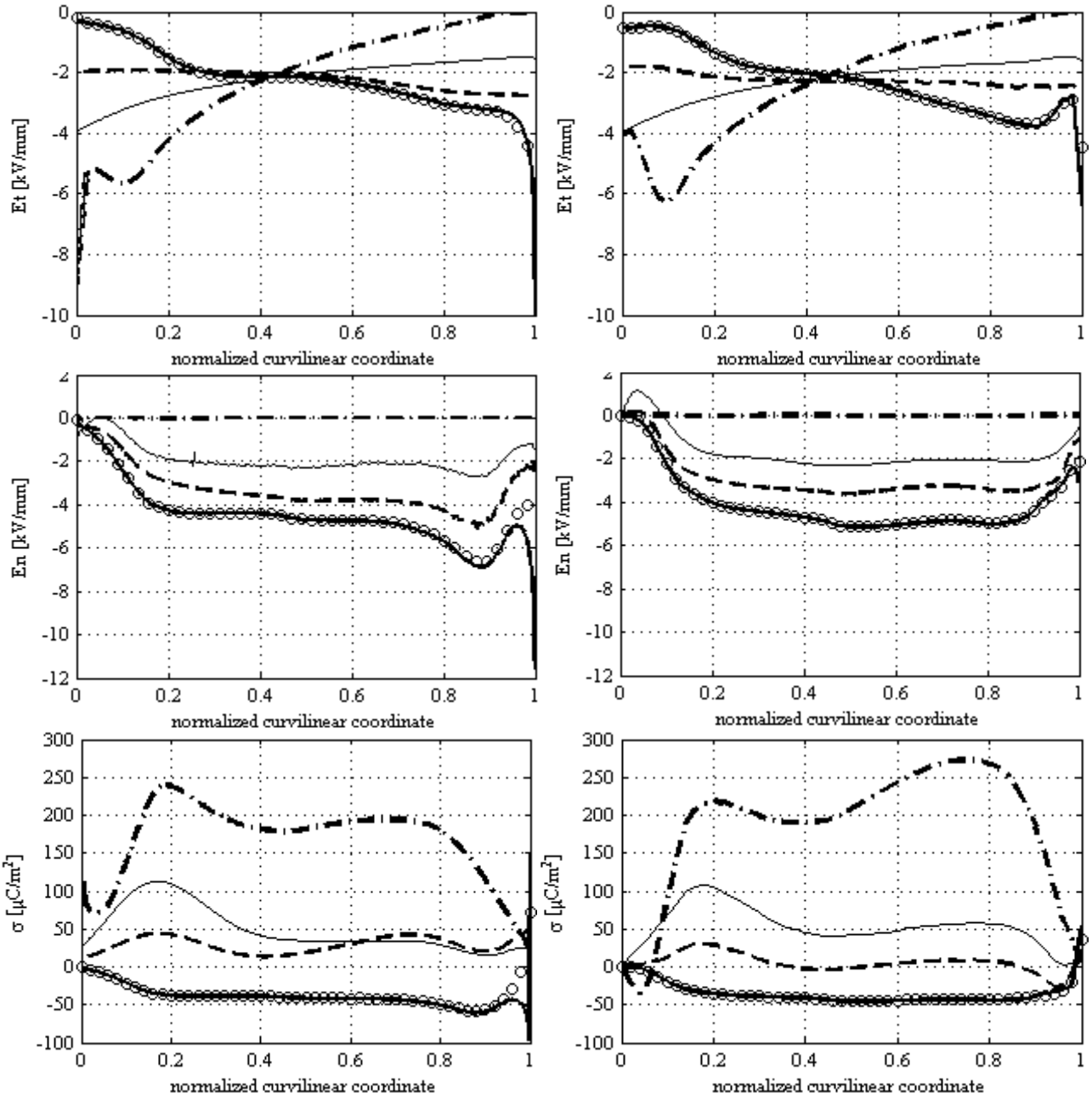

Figure 10. Comparison between reference spacer –left- and optimized spacer – right; upper surface
Case 1 Bold solid line, Case 2 solid line, Case 3 dashed line, Case 4 circle, Case 6 dash-dot line.

3.2.1.2 UPPER SURFACE

- Effects on electric field.
  - For all the cases there is an improvement of the normal electric field close to the outer conductor, especially for case 1; for case 2, 3, 4 E_n is slightly better along the surface.
  - Improvement of the tangential electric for cases 1 and 4 close to the outer conductor; case 6 improves instead at the inner electrode; for cases 2 and 4 the distribution remains unaffected; E_t for case 3 shows a reduction along the surface.
  - Effect on accumulated charge. Charge density decreases close to the outer conductor for case 1; case 2 and 4 remain almost unchanged and case 6 has a noticeable decrease of the accumulated charge close to the inner conductor; for the case 3 the charge is reduced almost to zero for one half of the spacer profile.

As for the lower profile, the most visible optimization effect on the charge accumulation has been obtained for cases 1 and 4, for which a reduction of both normal electric field and charge density has been obtained. This can be explained considering that for these cases the resistive electric field distribution does not greatly differ from the electrostatic distribution (i.e. the accumulated charge is relatively low in the reference spacer). For the other cases, in which there is a great difference between the conductivities (case 6) or great influence of the surface state (cases 2 and 3), the charge accumulation is not influenced by the optimization, and can be even larger.

As regards the upper profile, Figure 7 shows that the optimization produced only a moderate change near the outer electrode. As a matter of fact, the charge density remain almost unchanged for all the cases, apart case 3, for which the charge is reduced everywhere, in particular close to zero in the central part of the profile. This effect seems to be related to the reduction of the tangential electric field gradient, enhanced by the non linearity.

- Finally, it can be observed that the minimization of the electric field in the triple-junction region has always resulted effective in reducing the accumulated surface charge, even if such reduction

tends to increase the tangential electric field gradient near the electrodes.

4 CONCLUSIONS

The analyses performed on the post spacer model for the 1 MV transmission line of the ITER NBI system clearly indicate how strong is the influence of the conductivities in determining of the final surface charge distribution and, as a consequence, the final electric field distribution. These analyses also showed the very large variation of the surface charge setting up time constant, which can vary from few minutes to several days. These results show up the importance to have a good control of the insulation conductivities: for example, best results are obtained with "high" (with respect to SF6) epoxy bulk conductivity in presence of surface non linear conductivity. On the contrary, countermeasures like surface treatment addressed to increase the surface conductivity lead to an increase of surface charge accumulation, and an increase of the electric field in the critic region of the triple-junction. The case of enhanced SF6 conductivity is by far the worst case; actually, the RIC modeling with a uniform, very high conductivity of SF6 is certainly too rough for a precise assessment of the surface charge accumulation, so that efforts have to be devoted to a more detailed modeling of the RIC phenomenon.

From the point of view of the insulator designer, it is clear that identification of a method to produce "anti-charging" spacer profile is very welcome. The presented optimization method -applied to the disk spacer model- based on the minimization of the "surface charge drivers" E_n and ∇E_t, has given fair results for the cases in which the bulk epoxy conductivity is dominant with respect to the layer and SF6 conductivities; in the other cases, the optimization of the disk profile was not followed by a reduction of the surface charge. Finally, the minimization of the electric field in the triple-junction regions has been found always effective in reducing the surface charge.

5 REFERENCES

[1] www.iter.org

[2] ITER Document "DDD 5.3 Neutral Beam Heating & Current Drive (Nb H&Cd) System", IS N 53 DDD 29 01-07-03 R 0.1, 9 May 2005.

[3] T. Hasegawa, K. Yamaji, M. Sekita, J. Makino, J. Arai and K. Tada, "System design of Kii Channel HVDC link, CIGRE, No. 14-103, 1996

[4] T. Ohga, K. Usui, K. Ohmori, K. Watanabe, K. Ohshima, T. Itoh, M. Kawai and M. Kuriyama,"High voltage power supply of negative-ion based NBI for JT-60U", Fusion Engineering, 17th IEEE-NPSS Symposium, Vol. 2, pp.1091 - 1094, 1997.

[5] A. De Lorenzi, L. Grando, R. Gobbo, G. Pesavento, P.Bettini, R.Specogna and F.Trevisan, "The insulation Structure of the 1 Megavolt Transmission Line for the ITER Neutral Beam Injector", Fusion Engineering and Design 82, pp. 836–844, 2007.

[6] T. Hasegawa, F. Endo, K. Yamaji, T. Rokunohe, M. Hatano and T. Yamagiwa, "Development of Insulation Structure and Enhancement of Insulation Reliability of 500 kV DC GIS", IEEE Trans. Power Delivery, Vol. 12, pp. 194-202, 1997.

[7] T. Hasegawa, K. Yamaji, M. Hatano, H. Aoyagi, Y. Taniguchi and A. Kobayashi, "DC Dielectric Characteristics and Conception of Insulation for DC GIS", IEEE Trans. Power Delivery, Vol. 11, pp. 1776-1782, 1996.

[8] M. Shikata, K. Yamaji, M. Hatano, E. Tsuchie, H. Takeuchi and K. Inami, "Development and Design of DC GIS", Electrical Engineering in Japan, Vol. 129, pp. 51-61, 1999.

[9] E. Volpov, "Dielectric Strength Coordination and Generalized Spacer Design Rules for HVAC-DC SF_6 Gas Insulated Systems", IEEE Trans. Dielectr. Electr. Insul., Vol.11, pp. 949-963, 2004.

[10] K. Nakanishi, A. Yoshioka, Y. Arahata and Y. Shibuya, "Surface charging on epoxy spacers at dc stress in compressed SF_6 gas", IEEE Trans. Power Apparatus Syst., Vol. 102, pp. 3919-3927, 1983.

[11] C.X. Wang, A. Wilson and M.W. Watts, "Surface Flashover Sustained by Electrostatic Surface Charge on Epoxy Resin Insulator in SF_6", 6th Conf. Dielectric Materials, Measurements and Applications, Manchester, UK, pp. 182-185, 1992.

[12] B.M. Weedy, "DC conductivity of Voltalit epoxy spacers in SF6", IEE Proc. Part A, Vol. 132, pp. 450-454, 1985.

[13] D. C. Bassett, *Principles of polymer Morphology*, Cambridge University Press, UK, 1981.

[14] E. Volpov, "Electric Field Modeling and Field Formation Mechanism in HVDC SF_6 Gas Insulated System", IEEE Trans. Dielectr. Electr. Insul., Vol.10, pp. 204-215, 2003.
[15] E. Volpov, "HVDC Gas Insulated Apparatus: Electric Field Specificity and Insulation Design Concept", IEEE Electr. Insul. Mag., Vol.18, No.2, pp. 7-36, 2002.
[16] H. Fujinami, "Mechanism and Effect of DC Charge Accumulation on SF6 Gas Insulated Spacers", IEEE Trans. Power Delivery, Vol. 4, pp. 1765-1771, 1989.
[17] E.R. Hodgson and A. Moroño, "Radiation Effects on insulating gases for the ITER NBI system", J. of Nuclear Material, Vol. 258-263, pp. 1827-1830, 1998.
[18] E.R. Hodgson and A. Moroño, "A model for radiation induced conductivity in neutral beam injector insulator gases", J. Nuclear Material, Vol. 307-311, pp 1660-1663, 2002.
[19] Y. Fujiwara, M. Hanada, T. Inoue, K. Miyamoto, N. Miyamoto and Y. Ohara, "Radiation Induced Conductivity and Voltage Holding Characteristics of Insulation Gas for the ITER NBI", American Institute of Physics Conf. Proc. Vol. 439, pp. 205, 1998.
[20] D.E. Goldberg, "Genetic Algorithm in Search, Optimization and Machine Learning", MA, Addison-Wesley, 1989.
[21] A.J. Keane, "Genetic algorithm optimization of multi-peak problems: studies in convergence and robustness", Artificial Intelligence Engineering, Vol.9, pp. 75-83, 1995.
[22] P. Bettini and F. Trevisan, "Electrostatic Analysis for Plane Problems with Finite Formulation", IEEE Trans. Magnetics, Vol. 39, pp. 1127-1130, 2003.
[23] P. Bettini, E. Brusa, M. G. Munteanu, R. Specogna and F. Trevisan, "Static behaviour prediction of microelectrostatic actuators by discrete geometric approaches", IEEE Trans. Magnetics, Vol. 44, pp 1606-1609, 2008
[24] M.J.D. Powell, "Direct search algorithms for optimization calculations" Acta Numerica, Vol.7, pp. 287-336, 1998.

Antonio De Lorenzi (1958) received his degree in electrical engineering from the University of Padova, Italy, in 1984, In 1987 he received the post degree diploma from the School of Plasma and Controlled Thermonuclear Engineering at the same University.
Since 1984 he works as a researcher in the field of the Power Supplies for Thermonuclear Fusion Plants, in particular regarding the interaction with the EHV Grid and the pulsed power systems. Currently, he coordinates the researches on HVDC insulation in vacuum and gas for the 1 MV Neutral Beam Injector facility at Consorzio RFX, Padova, Italy.

Luca Grando (1972) received his Electric al Engineering degree from the University of Padova (I) in 1998 and the Ph.D. in electrical engineering from the same University in 2002. Currently, he is with Consorzio RFX, Padova, Italy, working in the research field of HVDC insulation in vacuum and gas for the 1 MV Neutral Beam Injector of ITER. His experience covers also the development of electric and magnetic diagnostic system and the devices for the active control of the MHD modes in thermonuclear plasma.

Alberto Pesce (1981) received his degree in electrical engineering from the University of Padova, Italy in 2006, cum laude. Currently he attends the doctoral school in Industrial Engineering at the same University. His research activities are in the field of HVDC isulation for the Neutral Beam Injectors for Thermonuclear Fusion Experiments, at Consorzio RFX, Padova, Italy.

Paolo Bettini (M'02) received the doctoral degree cum laude in electrical engineering from the University of Padova, Italy in 1994 and the Ph.D. degree in electrical engineering from the same University in 2002. From 1997 to 1999 he was with "Consorzio RFX" in Padova, Italy, where he worked on power supply and magnet systems of the RFX project. In 1999 he joined the University of Udine, Italy, as a researcher in Electrical Engineering. In January 2005 he became associate professor of Electrical Engineering at the same university. Presently he collaborates with national and international research groups and laboratories, working on applied electromagnetism and on fusion technology. He is author or co-author of over 50 scientific papers, mainly in the fields of analysis, synthesis and optimisation of electric and magnetic configurations, published in international journals or presented at international conferences.

Ruben Specogna (S'05-M'08) received the Master degree electronic engineering at the University of Udine, Italy, on April 2003. In 2007 he received the Ph.D. degree in electrical engineering from the University of Udine, Italy. In 2008 he become a researcher in Electrical Engineering in the same University. He is co-author of over 30 scientific papers, mainly in the fields of computational electromagnetism, published in international journals or presented at international conferences.